Acta Cryst. (1995). D**51**, 946–961

Human Class II MHC Molecule HLA-DR1: X-ray Structure Determined from Three Crystal Forms

BY JERRY H. BROWN*

Department of Biochemistry and Molecular Biology, and Howard Hughes Medical Institute, Harvard University, Cambridge, MA 02138, USA

THEODORE S. JARDETZKY

Department of Biochemistry and Molecular Biology, Harvard University, Cambridge, MA 02138, USA

LAWRENCE J. STERN

Department of Biochemistry and Molecular Biology, and Howard Hughes Medical Institute, Harvard University, Cambridge, MA 02138, USA

JOAN C. GORGA

Department of Pediatrics, Children's Hospital of Pittsburgh, Pittsburgh, PA 15213, USA

JACK L. STROMINGER

Department of Biochemistry and Molecular Biology, Harvard University, Cambridge, MA 02138, USA

AND DON C. WILEY†

Department of Biochemistry and Molecular Biology, and Howard Hughes Medical Institute, Harvard University, Cambridge, MA 02138, USA

(*Received* 15 *April* 1994; *accepted* 14 *February* 1995)

Abstract

The three-dimensional structure of the extracellular region of a 60 kDa class II major histocompatibility glycoprotein, HLA-DR1, was determined to 3.3 Å by X-ray crystallography using three crystal forms, each containing two molecules per asymmetric unit. Phases were initially determined to 4.2 Å using two crystal forms both containing DR1 from human lymphocytes complexed with a mixture of endogenous peptides. One of these crystal forms also contained a 28 kDa superantigen, *Staphylococcus aureus* enterotoxin B (SEB), bound to each DR1 molecule. Single-isomorphous replacement phasing followed by iterative two- and fourfold non-crystallographic real-space averaging between the two crystal forms resulted in 4.2 Å resolution electron-density maps from which the paths of the polypeptides could be traced. Cryocrystallography and synchrotron radiation were then used to extend the resolution to 3.3 Å for the two lymphocyte-derived crystal forms and for a third crystal form grown from DR1 produced in insect cells and complexed *in vitro* with a specific antigenic peptide. Iterative sixfold non-crystallographic real-space averaging resulted in an electron-density map into which 340 of 371 residues could be fit unambiguously. Crystal contacts and the existence of a parallel dimer of the DR1 $\alpha\beta$ heterodimer in the three crystal forms are discussed.

Introduction

The class II human leukocyte antigens (HLA) are 60 kDa glycosylated α,β heterodimeric products of the major histocompatibility complex (MHC) found on the surface of specialized cells of the immune system. Class II HLA presents peptides of $CD4^+$ helper T cells as part of the mechanism for identifying foreign antigens and initiating an immune response (Germain & Margulies, 1993). In humans, three class II MHC loci, DR, DQ and DP, are generally expressed. Both chains of the class II molecule include two extracellular domains (denoted α_1 and α_2, and β_1 and β_2 for the α and β chains, respectively), and short transmembrane and cytoplasmic portions. The β_1 domains in all three class II HLA families and the α_1 domains in DQ and DP are highly polymorphic in the human population. This polymorphism appears to contribute to variation in the immune response of

* Current address: Rosenstiel Basic Medical Sciences Research Center, Brandeis University, Waltham, MA 02254, USA.

† To whom all correspondence should be addressed.

ISSN 0907-4449

different individuals. Susceptibility or resistance to a number of diseases has been linked to particular alleles of the class II MHC (Nepom & Erlich, 1991).

To determine the structure of DR1, a common HLA-DR haplotype, the membrane anchor and cytoplasmic domains were first removed. This was accomplished by papain digestion of DR1 that had been purified in detergent from cultured human lymphoblastoid cells (Gorga, Horejsí, Johnson, Raghupathy & Strominger, 1987). After a large-scale purification for the soluble protein was developed (Gorga *et al.*, 1987), a number of DR allelic variants were crystallized (Gorga, Brown, Jardetzky, Wiley & Strominger, 1991), including the DR1 reported here. Elution of peptides bound to the DR1 used in the first two crystal forms indicates that a mixture of endogenous sequences from 12 to 24 amino acids long are present (Chicz *et al.*, 1992). The third crystal form was grown from a soluble version of DR1 heterologously expressed in baculovirus-infected Sf9 insect cells and

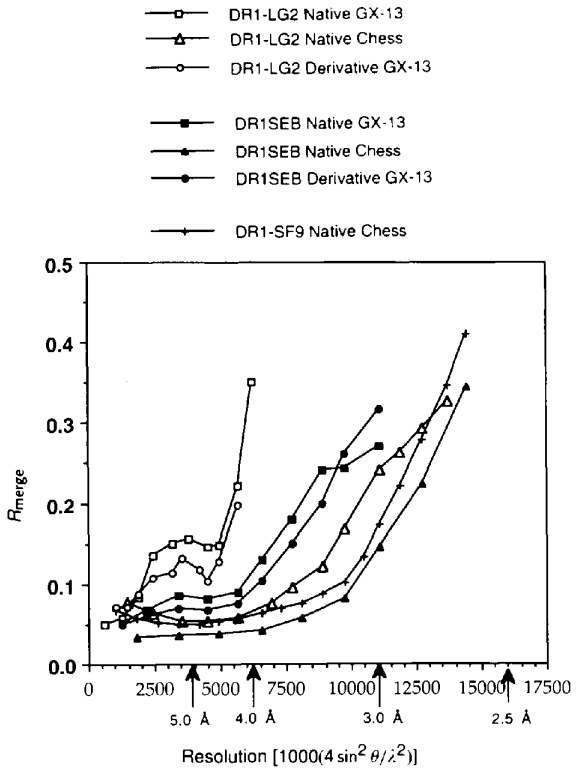

Fig. 1. Data quality as a function of resolution (Å). (*a*) $R_{merge} = (\sum_{hkl}\sum_{obs}|I^{hkl}_{obs} - \langle I^{hkl}\rangle|)/(\sum_{hkl}\sum_{obs} I^{hkl}_{obs})$. (*b*) Fraction complete = (number of independent reflections)/(maximum number theoretical).

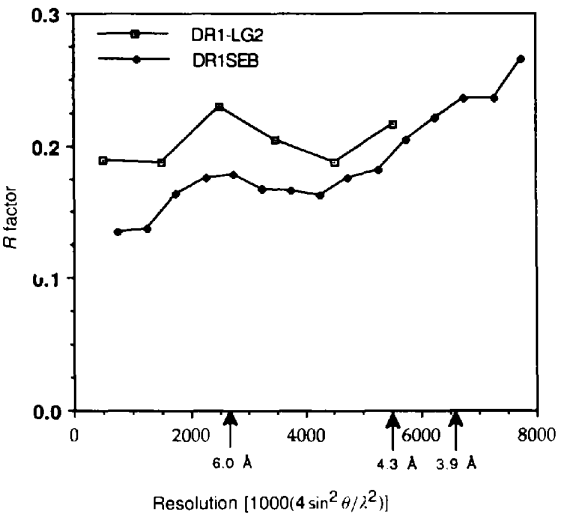

Fig. 2. The *R* factor between the native and derivative data sets as a function of resolution (Å) as determined by the *CCP4* (Collaborative Computational Project, Number 4, 1994) program *RSTATS*. $R = \sum|F_{Native} - F_{HgDer}|/\sum F_{Native}$.

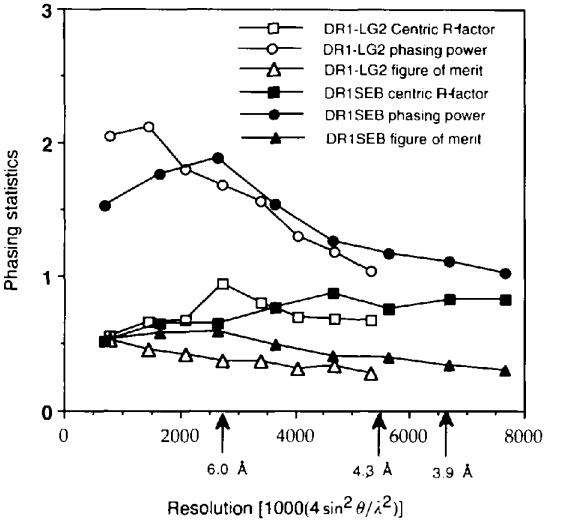

Fig. 3. The statistics of Table 3, as a function of resolution.

complexed with a single peptide from the influenza virus haemagglutinin (Stern & Wiley, 1992). The DR1 structure (Brown *et al.*, 1993) is similar to that of the class I MHC molecule (Bjorkman *et al.*, 1987*a*,*b*), and to a hypothetical model of the class II peptide binding site (Brown *et al.*, 1988). Clear electron density representing the mixture of peptides in lymphocyte DR1 indicates that peptides of different sequences bind with similar elongated conformations (Brown *et al.*, 1993). A number of residues conserved in class II molecules make 12 hydrogen bonds to backbone atoms of the influenza haemagglutinin peptide bound to DR1 providing a universal mechanism for peptide recognition (Stern *et al.*, 1994) different from that observed in class I MHC molecules (Madden, Gorga, Strominger & Wiley, 1991, 1992; Madden & Wiley, 1992; Madden, Garboczi & Wiley, 1993; Zhang, Young, Imaraí, Nathenson & Linsley, 1992; Fremont, Matsumura, Stura, Peterson & Wilson, 1992; Silver, Guo, Strominger & Wiley, 1992; Guo *et al.*, 1992).

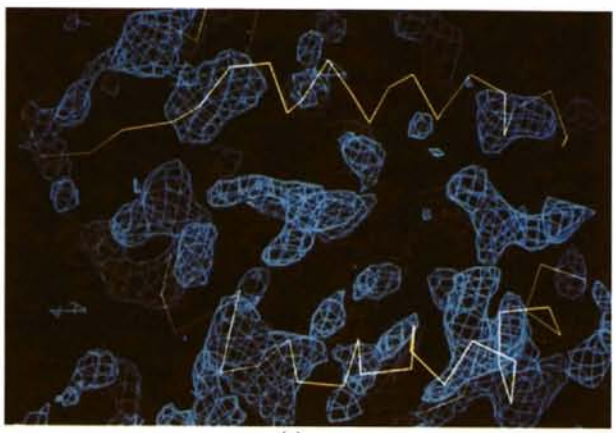

(*a*)

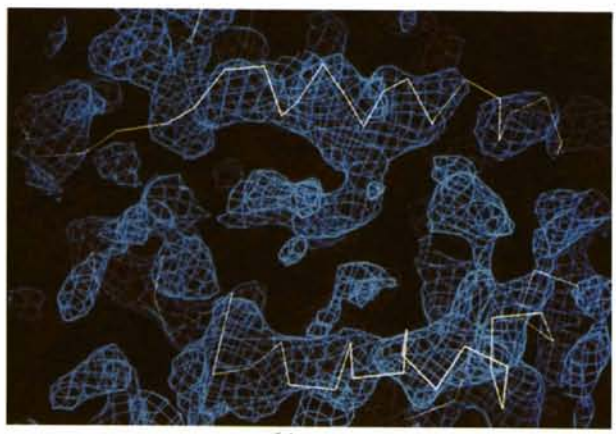

(*c*)

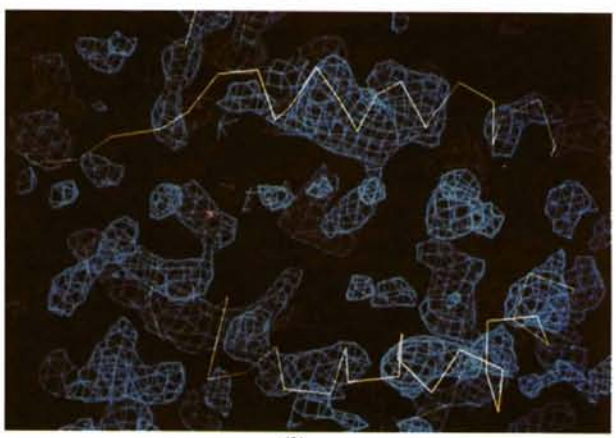

(*b*)

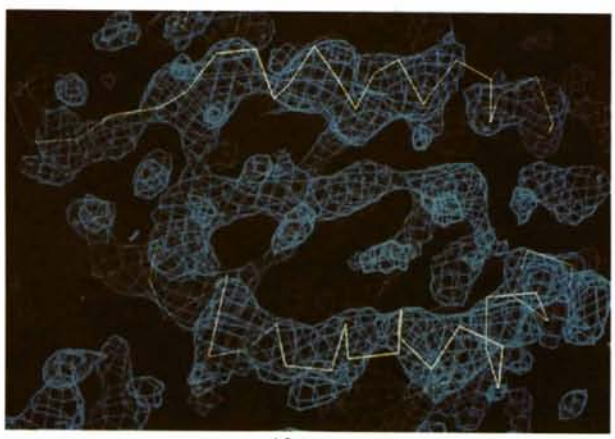

(*d*)

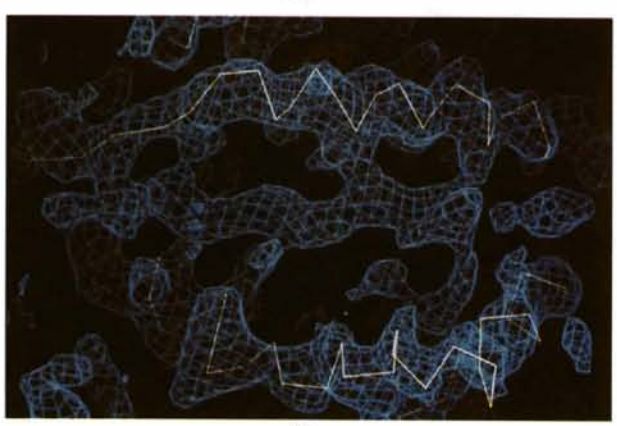

(*e*)

Fig. 4. Progression of the 4.2 Å electron-density maps at various stages of real-space averaging. All maps (blue) are contoured at 2σ. The model (yellow) is the Cα coordinates of DR1 displayed using *FRODO* (Jones, 1978). The helical regions (α on top, β on bottom) of the antigen-binding site are shown. The density between the helices is from bound peptides. (*a*) DR1-LG2 F_{obs}, φSIR. (*b*) DR1SEB F_{obs} φSIR/ANO. (*c*) Simple 'twofold' average of the above two maps (no iteration) according to the transformation in Fig. 5(*a*). (*d*) Iteratively 'twofold' averaged map (also see Figs. 7 and 8). (*e*) Iteratively 'fourfold' averaged map (also see Fig. 10).

Table 1. *Data sets used for the* 4.2 Å *(top four sets of rows) and* 3.3 Å *(bottom three sets of rows) structure determinations*

All crystals contain two DR1 heterodimers per asymmetric unit. Unit-cell standard deviations are ≃ 0.3 Å; the DR1(LG-2) *c* dimension, however, is less accurate, e.s.d. ≃ 1.4 Å.

X-ray source* Temperature (K)	Protein (Source)†	Space group	Unit cell *a*, *b*, *c* (Å)	Derivative	Limiting resolution (Å)
GX-13 277	DR1(LG-2)	$C222_1$	96.7 112.6 209	Native	4.0
GX-13 277	DR1(LG-2)	$C222_1$	96.6 112.6 209.2	K_2HgI_4	4.2
GX-13 108	DR1(LG-2) SEB	$P2_12_12_1$	95.7 115.9 150.4	Native	3.4
GX-13 108	DR1(LG-2) SEB	$P2_12_12_1$	95.9 117.1 150.8	K_2HgI_4	3.2
CHESS 103	DR1(LG-2)	$C222_1$	96.7 114.4 216.8	Native	2.7
CHESS 103	DR1(LG-2) SEB	$P2_12_12_1$	95.0 114.7 149.8	Native	2.7
CHESS 103	DR1(SF9) HA306–318	$P4_32_12$	95.4 95.4 245.7	Native	2.75

* CHESS = Cornell High Energy Synchrotron Source, GX-13 = Elliot rotating anode.

† SEB source: SEB used in these frozen crystals was a kind gift of M. Sax, VA Medical Center, Pittsburgh, PA. The same crystals were also obtained from SEB purchased from Toxin Technology Inc., Sigma, or purified from an SEB producing strain of *S. aureus*. LG-2: human lymphoblastoid cell line (Gorga *et al.*, 1987). Sf 9: *Spodoptera fragiperda*, insect cell line infected with recombinant baculoviruses (Stern & Wiley, 1992). HA306–318: influenza virus haemagglutinin peptide sequence number 306–318.

Here we report how the DR1 structure was determined from X-ray diffraction data of three crystal forms containing DR1, although one form also contained a 28 kDa superantigen protein bound to DR1 (Jardetzky *et al.*, 1994) and another form contained DR1 expressed in insect cells with a different bound peptide and different oligosaccharide structures (Stern & Wiley, 1992).

Structure determination at 4.2 Å

Data collection and processing

Crystals of DR1 isolated from the human *B* lymphoblastoid cell line LG-2 (DR1-LG2) were first obtained from high salt conditions, *e.g.* 28% PEG 3350, 2.0 *M* NaCl, in the space group *C*222 or $C222_1$, $a = 144$, $b = 222$, $c = 61$ Å (Brown, 1991), but were highly mosaic (*ca* 2° full-width rocking curve) and diffracted to low resolution. Two other crystal forms, grown under similar conditions, were used for the initial DR1 structure determination at 4.2 Å. First, crystals of DR1-LG2 suitable for structure determination (mosaic spread *ca* 0.5°) (Table 1, Fig. 1) were initially grown at pH 4.0 (by TSJ) and later at pH 5.5–6.0 from 27% PEG 8000, 0.1 *M* Glycine, 0.01% NaN_3, 0.05 *M* MES in the space group $C222_1$ $a = 96$, $b = 112$, $c = 209$ Å. With two DR1 molecules per asymmetric unit, this crystal form contains 54% solvent; at the stage of space-group determination, however, we were not yet able to rule out the possibility of a high-solvent crystal with only one molecule in the asymmetric unit. The second crystal form contains the superantigen *Staphylococcus aureus* enterotoxin B (SEB) in 1:1 complex with DR1 (space group = $P2_12_12_1$ $a = 96$, $b = 116$, $c = 150$ Å) and was grown using the same human lymphocyte derived DR1 mixed with SEB further purified by gel filtration as has been described in detail elsewhere (Jardetzky *et al.*, 1994).

Native and derivative X-ray data (Table 1, first four sets of rows) were collected from the DR1-LG2 and DR1SEB crystals with a Xentronics area detector (Durbin *et al.*, 1986) using an Elliott GX-13 X-ray source focused with Franks mirrors (Harrison, 1968), then integrated and scaled using the *BUDDHA* (Blum, Metcalf, Harrison & Wiley, 1987) and *CCP*4 (Collaborative Computational Project, Number 4, 1994) programs.

Rotation function attempts

In spite of the predicted similarity between class II and class I MHC molecules (Kaufman, Auffray, Korman, Shackelford & Strominger, 1984; Brown *et al.*, 1988) we were unsuccessful in using molecular replacement to solve the DR1 structure. The class I molecule, HLA-A2, is comprised of a superdomain (α_1 and α_2) with a groove containing the bound peptide (Bjorkman *et al.*, 1987*a*,*b*; Saper, Bjorkman & Wiley, 1991) and two immunoglobulin-like domains (β_2m and α_3). These correspond to

the class II α_1, β_1, α_2 and β_2 domains, respectively. Cross-rotation functions were calculated between the Patterson functions of the DR1-LG2 native GX-13 X-ray data (Table 1, line 1) and of a hypothetical class II HLA-DR1 model derived from the HLA-A2 crystal structure (Saper *et al.*, 1991) by substituting in DR1 side chains according to published sequence alignments (Brown *et al.*, 1988; Brown, 1991). Using data from 8 to 4.2 Å and a Patterson integration radius of 25 Å, various models were tested with the *MERLOT* programs (Fitzgerald, 1988). Putative rotation-function (Crowther, 1972) solutions were tested with translation functions (Crowther & Blow, 1967) and rotation-function refinement (Brünger, 1990). No combined rotation translation solution was discovered that could produce interpretable electron-density maps. In retrospect, after the structure was determined, it was clear that a rotation-function peak of 3.83σ (Table 2, SET 1, peak 2) had been found very near the correct value (25, 85, 0°) when the β_2 domain and the 102 least certain modeled residues of the 271 residues in α_1, α_2 and β_1 were omitted from the search model (Table 2, set 1, see headnote). [In the final DR1 model, β_2 is offset significantly compared to the homologous (α_3) domain in class I MHC (Brown *et al.*, 1993).] In an identical calculation including the β_2 domain the eighth highest peak of 3.16σ (Table 2, set 2, peak 8) is near the correct solution. Attempts to refine these observed rotation-function solutions (Brünger, 1990) did not succeed, possibly because the observed peaks were very broad and the correct solution is found at one edge of the peak. When other single domains were removed and the least certain residues were included in the model no peak above 2.5σ was found at the correct position.

The DR1 crystal was eventually shown (see below) to contain two DR1 molecules per asymmetric unit related by an approximate twofold axis (Brown *et al.*, 1993). However, no significant rotation-function peaks were found corresponding to the second molecule (expected $\alpha = 4$, $\beta = 46$, $\gamma = 114°$). In retrospect, the absence of such peaks may have been caused by the second molecule being less well defined in the final model: it has a higher average *B* factor, poorer peptide electron density, and its mercury heavy-atom isomorphous derivative refined to a lower occupancy (Table 3).

Table 2. *Cross-rotation function between the Patterson functions of the hypothetical DR1 model and the DR1-LG2 native X-ray data*

At 8–4.2 Å resolution (Table 1, line 1) with a cutoff radius of 25 Å, using the program *MERLOT* (Fitzgerald, 1988). The hypothetical class II model of the α_1, α_2, β_1 and β_2 domains were derived from the class I HLA-A2 α_1, β_2m, α_2, and α_3 domains, respectively. Only confidently aligned residues (Brown *et al.*, 1988; Brown, 1991) were included. Full side chains were used. Different parts of the model were used '+' indicates the domain was included in the model, '−' indicates that it was omitted. The bottom angles of each set indicate the true solution. Euler angles defined as an $\alpha°$ rotation about the *Z* axis, a $\beta°$ rotation about the new *Y* axis, and a $\gamma°$ rotation about the new *Z* axis. The rotation space was sampled from 0–90° by 5° in β, 0–360° by 5° in γ, and 0–180° by 2.5° in α (Rao, Jih & Hartsuch, 1980).

Domains included				Peak				Peak
α_1	α_2	β_1	β_2	No.	α	β	γ	/r.m.s.
Set 1								
+	+	+	−	1	57.5	80.0	10.0	4.92
				2	35.0	85.0	355.0	3.83
				3	145.	90.0	180.0	3.81
					25.0	85.	0.0	3.39
Set 2								
+	+	+	+	1	67.5	70.	10.0	4.58
				2	92.5	90.	250.	3.33
				3	87.5	90.	70.0	3.33
				8	35.0	90.0	355.	3.16
					25.0	85.	0.0	<3.0

Heavy-atom derivative

Having been unable to derive useful phase information from molecular replacement, we then pursued experiments in isomorphous replacement. DR1-LG2 crystals were soaked in 35 heavy-atom solutions, and DR1SEB crystals were soaked in 20 solutions. The crystals were examined either by precession photographs or Xentronics area detector data collection (Brown, 1991, and unpublished work). One heavy-atom solution, 0.12 m*M* K_2HgI_4, 0.3 m*M* KI soaked overnight, yielded an interpretable difference Patterson map with two sites per asymmetric unit in both crystal forms. In the DR1SEB crystal, PCMBS gave a similar set of differences. (The heavy metal binds to the molecule's only free cysteine, at β30 in the peptide-binding groove, although this was not known until the structure was solved.) Heavy-atom refinement statistics are described in Figs. 2 and 3, and Table 3.

Single isomorphous replacement (SIR) and SIR/anomalous electron-density maps from the heavy-atom data were calculated for DR1-LG2 (Fig. 4*a*) and DR1SEB (Fig. 4*b*), respectively. These maps were not of sufficient quality for model building; however, they were significantly improved by the technique of non-crystallographic averaging (Bricogne, 1976). In order to average the two electron-density maps, first a transformation relating DR1 in the DR1-LG2 crystal form to the DR1 in the DR1SEB form had to be calculated. Following the simple averaging, molecular envelopes were required to allow iterative real-space phase averaging (Bricogne, 1976).

Transformation relating DR1-LG2 and DR1SEB crystals

The initial determination of the transformation relating the DR1-LG2 space group to the DR1SEB space group (Fig. 5*a*) was facilitated by the presence of two mercury peaks per asymmetric unit the same distance apart, *ca* 27.5 Å, in both space groups. We inferred from the identical inter-mercury distances that the conformation of the molecule(s) in this region of the map were similar for the two crystal forms. (Only later did we discover that

Table 3. *Heavy-atom refinement statistics*

The program *HEAVY* (Terwilliger & Eisenberg, 1983) was used to refine the heavy-atom parameters against the origin-removed Patterson map based on 317 centric reflections. A phase shift of 90° was applied to *h*0*l* reflections with l = odd (*International Tables for Crystallography*, 1965). Form factors for Hg^{2+} were used. 20 cycles of refinement of occupancies and positions were followed by 20 cycles of isotropic temperature factors and positions, and another 20 cycles of occupancies and positions. This was followed by minimization of lack of closure at the best phase. The positions and occupancies of the heavy atoms converged within 20 cycles. B converged to within 0.002σ. The phasing power and centric R factor are defined as follows: phasing power = r.m.s. (f_{Hg})/r.m.s.(E), centric R factor = $(\sum_h^{kl} ||F_{HgDer} - F_{Native}| - f_{Hg}|)/(\sum |F_{HgDer} - F_{Native}|)$ where F_{HgDer} and F_{Native} are the observed derivative and native amplitudes, f_{Hg} is the calculated mercury amplitude, and E is the residual lack of closure. The phasing power listed is calculated with acentric data. The centric R factor is calculated with the centric data. Similar procedures were used for the refinement of the heavy atom in the DR1SEB crystal form (Jardetzky *et al.*, 1994).

Crystal	Hg site	Occupancy	(Fractional) X	Y	Z	B	Phasing power	Centric R factor	Figure of merit
DR1-LG2	1	2.186	.0457	.0997	.1033	36.7	1.49	0.70	0.37
	2	1.770	.1369	.1631	.2246	33.2			
DR1SEB	1	0.936	.9248	.9621	.7702	1.17	1.32	0.71	0.44
	2	0.810	.8327	.0261	.9335	4.57			

both crystals contained two DR1 molecules per asymmetric unit.) Thus, a one-dimensional real-space correlation search between the two electron-density maps around the Hg–Hg axis was calculated instead of a six-dimensional real-space correlation search, in order to determine the transformation between the crystals.

A 6 Å resolution DR1-LG2 SIR electron-density map was calculated in sections perpendicular to the Hg1–Hg2 axis, with the origin at Hg1. DR1SEB electron-density maps skewed the same way and, alternatively, skewed with Hg2 as the origin ('switched') were compared within a cylinder around the Hg1–Hg2 axis using *CYLINDER* (Metcalf, Blum, Freymann, Turner & Wiley, 1987). The correlation coefficient as a function of the angular search around the cylinder axis is plotted in Fig. 5(*a*). The highest peak (at ~ 100° in the 'switched case') suggested that Hg1 in DR1-LG2 corresponds to Hg2 in DR1SEB and defines a transformation matrix (Fig. 5*b*), which was refined further by iteratively refining the cylinder axis to within 0.5°. [The second peak (at ~ −120° in the 'direct' correlation, Fig. 5*a*), however, suggests that Hg1 in DR1-LG2 also corresponds to Hg1 in DR1SEB, indicating in retrospect the existence of a dimer of DR1 molecules per asymmetric unit in both

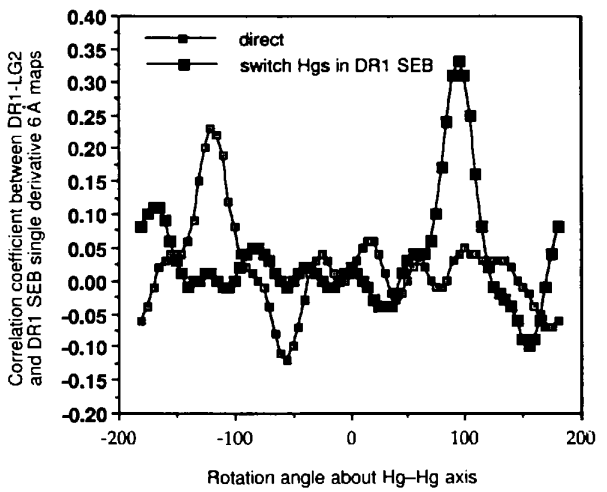

(*a*)

$$R_{DR1\text{-}LG2 \Rightarrow DR1SEB} = \begin{pmatrix} .9994 & -.0213 & .0256 \\ -.0046 & -.8506 & -.5256 \\ .0329 & .5252 & -.8503 \end{pmatrix}$$

$$T = \begin{pmatrix} 25.7 \\ 108.4 \\ 73.4 \end{pmatrix}$$

(*b*)

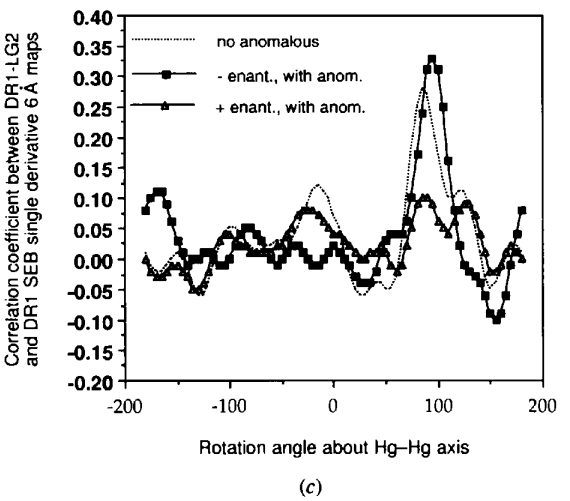

(*c*)

Fig. 5. (*a*) Real-space correlation coefficients between the DR1-LG2 SIR electron-density map and the DR1SEB SIR/ANO electron-density map as a function of angle (°) around the common Hg1 to Hg2 axis. Correlation within a cylinder 57 Å long and 15 Å radius calculated by *CYLINDER* (Metcalf *et al.*, 1987). (*b*) Initial transformation relating the electron density between the DR1-LG2 and DR1SEB crystals. (*c*) Real-space correlation coefficients between the '−enantiomorph' DR1-LG2 SIR map and −enantiomorph DR1SEB SIR map (dotted line), between the −enantiomorph DR1-LG2 SIR map and the −enantiomorph DR1SEB SIR/anomalous map (square box), and between the +enantiomorph DR1-LG2 SIR map and the +enantiomorph DR1SEB SIR/anomalous map (triangle).

crystal forms (see below).] These correlation peaks also established that the DR1-LG2 and DR1SEB phase sets were in reference to a common enantiomorph. The absolute hands of the electron-density maps were determined by comparing the correlation coefficients between the DR1-LG2 and DR1SEB maps with and without anomalous-scattering contribution (square-box and dotted curves in Fig. 5*c*).

Envelope construction

With the initial transformation relating electron density in the DR1-LG2 and DR1SEB crystals (Fig. 5*b*), the two maps from the two crystals were averaged. In addition to showing more recognizable electron-density features (Fig. 4*c*), this map allowed an envelope to be drawn (Fig. 6) around the strong electron density common to both maps, *i.e.* the DR1 (later shown to be two DR molecules). The moderate density remaining in the DR1SEB SIR/ANO map was assigned to an SEB envelope. Envelopes were initially drawn on a 2 Å grid and then transferred [using *GENERATE* (mode 3) and *RECNV6* (Bricogne, 1976)] to a 1 Å grid. [The Bricogne averaging algorithm (Bricogne, 1976) creates sorted lists of grid points from the contents of the envelopes so that only relatively small regions of the electron-density map need be kept in computer memory at any one time.]

Iterative twofold averaging

Iterative twofold averaging between the two crystals followed procedures described previously (Saper *et al.*, 1991; Loebermann, Tokuoka, Deisenhofer & Huber, 1984) where in each cycle electron-density maps are averaged in each of the crystal frames. Averaging between DR1-LG2 and DR1SEB required reconstruction of maps averaged within the DR1 envelope and unaveraged within the SEB envelope. This posed no problem in the DR1-LG2 frame (the left-hand portion of Fig. 7, excluding programs marked with a † which are used for fourfold averaging described later in the text). DR1 densities were fetched from the DR1SEB map and averaged with the DR1 densities from the DR1-LG2 map (using Bricogne's *MODIFY*). Every point in the DR1 envelope had a partner in the DR1SEB map and was thus averaged. In the DR1SEB frame (right-hand portion of the flow chart, Fig. 7), a portion of the crystal contents, *i.e.* the SEB, did not have a partner in the DR1-LG2 crystal. Two lists were generated: one containing all the non-solvent densities within the DR1SEB map, the other containing only those points within the DR1 portion of the map brought from the DR1-LG2 frame. These lists were appended (program written by TSJ) and the maps 'averaged' using Bricogne's *RECONSTITUTE*. At this initial stage, averaging only the asymmetric units of the two crystals, the DR1 portion of the map became twofold averaged whereas the SEB portion was simply passed along.

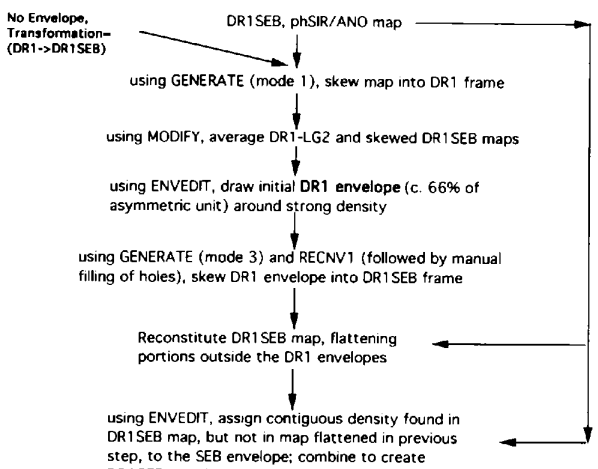

Fig. 6. Schematic of procedure used to draw the initial DR1 and DR1SEB envelopes. All programs are from *CCP*4 (Collaborative Computational Project, Number 4, 1994) or *Joy of Skewing* (Bricogne, 1976) unless otherwise noted. [The relatively smaller envelope, as a percent of the asymmetric unit, used in the DR1SEB space group as compared to the DR1-LG2 space group is probably due to initial omission of weak SEB electron density (Jardetzky *et al.*, 1994) from the envelope.]

The 4.2 Å resolution map resulting from iterative twofold real-space averaging to convergence (Fig. 8) was of sufficient quality to identify the domains of the HLA structure. For example, the regions of the map corresponding to the peptide-binding domains (Fig. 4*d*) show largely continuous electron density for the helices of the α_1 and β_1 domains as well as for the mixture of endogenous peptides in-between. Electron density of similar quality was also observed for the immunoglobulin-like α_2 and β_2 domains.

This twofold iteratively averaged electron-density map furthermore showed that two DR1 molecules were found in the asymmetric units of both crystals. To date, all crystal forms of DR1 have been found to contain two molecules per asymmetric unit in an approximately twofold symmetric dimer (see the discussion below).

Transformation between heterodimers in the dimer of dimers

The identification of a non-crystallographic dimer of DR1 α,β heterodimers in both the DR1-LG2 and DR1SEB crystals made fourfold averaging possible. The transformation between the electron density in the DR1-LG2 and DR1SEB crystals was redefined (Fig. 9, M1) by choosing a different cylindrical portion of the map that more fully overlapped the DR1 molecules, with the cylinder axis coincidental with the dimer axis. A correlation search on this part of the DR1-LG2 SIR map at 4.2 Å yielded a transformation 2.2° and 3.0 Å different from the one described in Fig. 5(*b*) and resulted in a twofold averaged map (between DR1-LG2 and

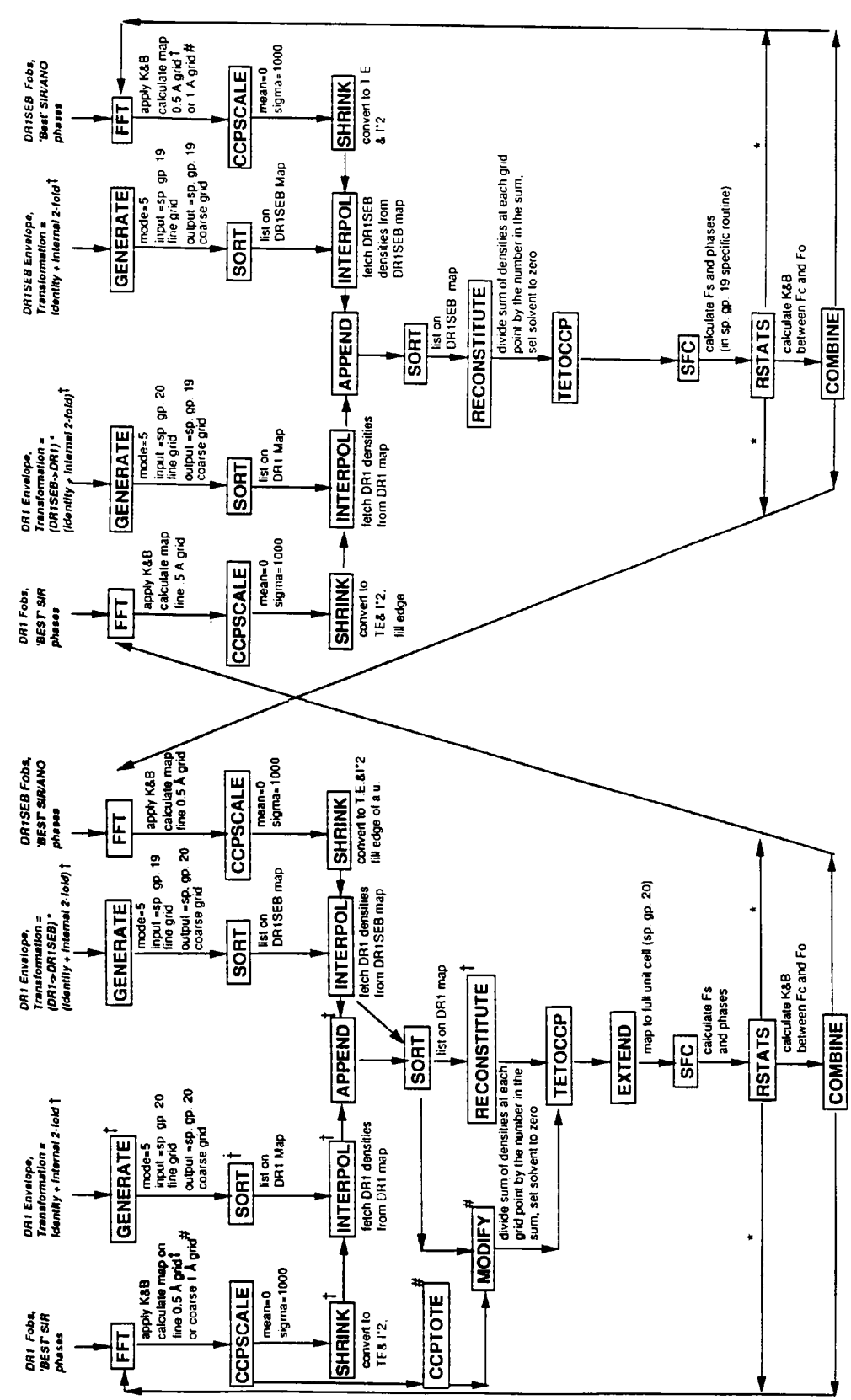

Fig. 7. The flow chart of programs used to iteratively average electron-density maps between the DR1-LG2 ($C222_1$, space group 20) crystal form and the DR1SEB ($P2_12_12_1$, space group 19) crystal form. For each cycle, maps are averaged both in the $C222_1$ DR1-LG2 frame (left half) and in the $P2_12_12_1$ DR1SEB frame (right half). The programs in boxes are either from *CCP4*, *Joy of Skewing* (Bricogne, 1976), or unpublished work. † indicates input or programs used only for the fourfold averaging, # only for twofold averaging, * only for Sim-weighted $2F_o - F_c$ phase cal map. Abbreviations used: K and B are scale and temperature factors, TE is Ten Eyck format electron-density map, F_c and F_o are calculated and observed structure factors.

DR1SEB) with improved connectivity at the 'bottom' of the immunoglobulin-like domains.

Transformations relating the two DR1 heterodimers within the asymmetric units of both crystals were defined using one-dimensional real-space correlation searches (Fig. 9, M2, M3). From a preliminary C^{α} model of each DR1 molecule, a local coordinate axis was defined from the Hg atom at Cysβ30 to the C^{α} atom at residue α95. After superimposing these axes from two DR1 molecules, an electron-density correlation search around the axes was calculated using *CYLINDER* (Metcalf *et al.*, 1987). The relationship between the two DR1 molecules

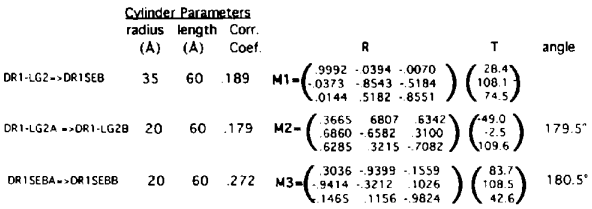

Fig. 9. Redetermination of the transformation between the DR1-LG2 and DR1SEB crystals (first line) and determination of the transformations between the two DR1 molecules per asymmetric unit in each crystal (second and third lines) that allowed fourfold averaging to be performed. The maps used were calculated to 4.2 Å but are otherwise the same DR1-LG2 SIR and DR1SEB SIR/ANO maps used in Fig. 5(*a*).

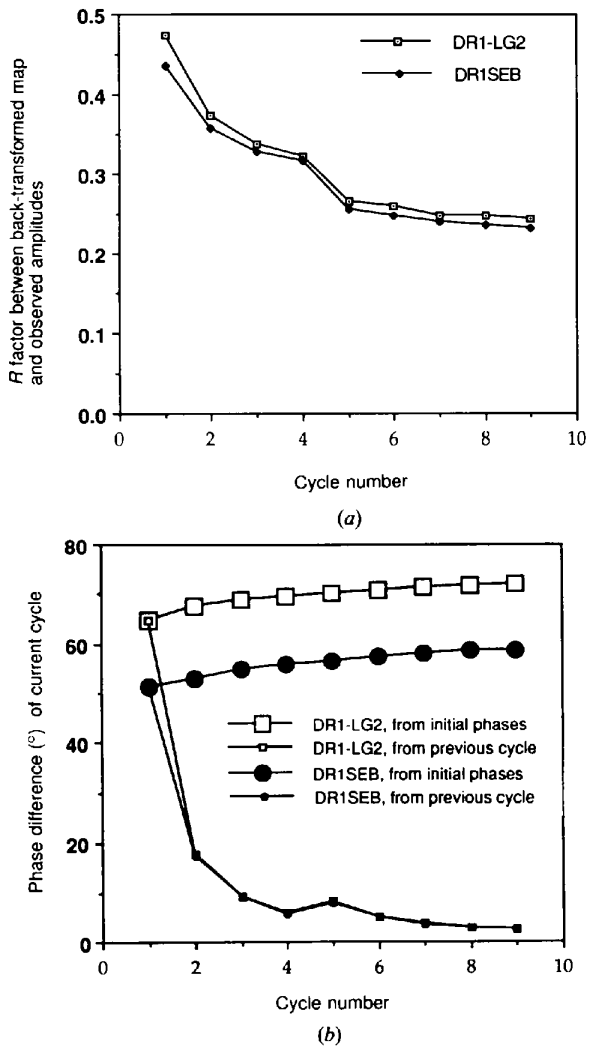

Fig. 8. (*a*) Statistics from the first 'twofold' 4.2 Å resolution averaging experiment between the DR1-LG2 crystal form and the DR1SEB crystal form. DR1 density is twofold averaged, SEB density is not averaged. Input for the FFT-calculated maps are initially observed structure factors (F_{obs}) and 'best' isomorphous phases. Input for cycles 2–4 include F_{obs} and combined phases (φ_{comb}). Input for cycles 5–9 include combined structure factors (Stuart & Artymiuk, 1985) and φ_{comb}. $R = \sum_{hkl} |F_{observed} - F_{calculated\ from\ averaged\ map}| / \sum_{hkl} F_{observed}$. (*b*) Phase changes in the DR1-LG2 and DR1SEB crystal frames in the first 'twofold' averaging experiments.

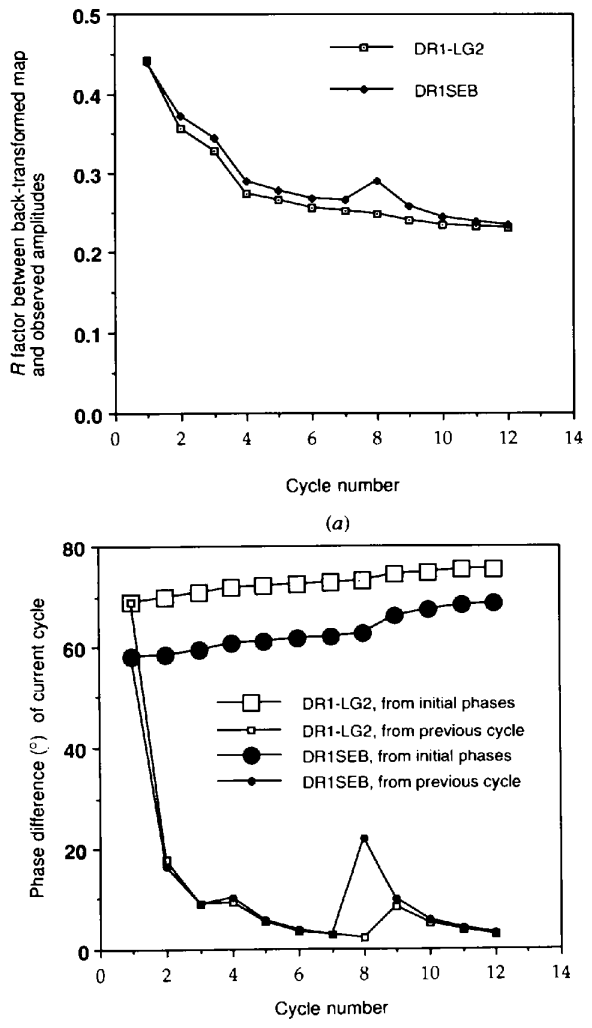

Fig. 10. (*a*) Statistics from the first 'fourfold' 4.2 Å resolution averaging experiment. DR1 electron density is fourfold averaged. The discontinuity in the DR1SEB *R* factor is due to the introduction of twofold averaging of the SEB density starting at cycle 8. FFT-input is similar to the 'twofold' averaging described in Figs. 7 and 8 except the input to cycles 9–13 includes Sim-weighted $2F_{obs} - F_{calculated}$ coefficients and calculated phases. (*b*) Phase changes in the first fourfold averaging experiments.

in the asymmetric unit was found to be nearly a 180° rotation (Fig. 9). (This inter-heterodimer relationship is *ca* 175–178° for a third DR1 space group described later.)

Iterative fourfold averaging

The iterative averaging procedure used to fourfold average DR1 electron density and twofold average SEB electron density (Fig. 7, including programs and input designated by a †) is very similar to the procedure used to twofold average DR1 electron density explained above. The fourfold averaging procedure was iterated for a total of 13 cycles to convergence (Figs. 10*a* and 10*b*). The *R* factors between the back-transformed, final averaged map and the DR1-LG2 and DR1SEB data sets are 23.0 and 23.4%. A preliminary atomic model of the structure was built into the iteratively fourfold averaged electron-density map, where, for example, the ridges in the helical electron density were first observed (Fig. 4*e*).

Structure determination at 3.3 Å

At this stage in the structure determination a third crystal form of DR1 became available. DR1 for this form was expressed as a soluble heterodimer in Sf9 insect cells (DR1-SF9), purified as an empty molecule, and subsequently complexed with the 13-residue influenza virus peptide HA 306–318. It crystallized in the space group $P4_32_12$ $a = 95$, $b = 95$, $c = 247$ Å from 15% PEG 8000, 0.02% NaN_3, 100 m*M* sodium acetate, pH 4.6 (Stern & Wiley, 1992). Native X-ray data for DR1-SF9 as well as for DR1-LG2 and DR1SEB were then collected on phosphor image plates at CHESS with 0.91 Å wavelength X-rays and integrated using *DENZO* (Z. Otwinowski, personal communication) from crystals that had been soaked in cryoprotectant (Table 1, row sets 5–7), mounted in Nichrome (DR1SEB) or glass (DR1-LG2 and DR1-SF9) loops (Teng, 1990) and flash cooled to 108 K in a stream of cold nitrogen. This resulted in approximately 1 Å improvement in resolution over that obtained with the laboratory X-ray source (GX-13) at 277 K (Fig. 1*a*). The glass loops, being much thinner and transparent to X-rays, permitted collection of data obscured by Nichrome loops, and allowed measurement of nearly 100% of the data (Fig. 1*b*).

The 4.2 Å model of the DR1 dimer of α,β heterodimers was rotated and translated into the asymmetric units of the cryogenic DR1-SF9 data set (Stern *et al.*, 1994) as well as the cryogenic data sets of DR1-LG2 and DR1SEB by molecular replacement using *MERLOT* (Fitzgerald, 1988) followed by rigid-body refinement using *X-PLOR* (Brünger, 1992) where individual domains were allowed to move as rigid bodies. Molecular envelopes were redrawn using *ENVATOM* (Harrison, 1968) or *ENVTOM* (Garrett, Saper, Bjorkman, Strominger & Wiley, 1989) by including grid points within 4 Å of model coordinates. Transformations between the six DR1 molecules of the three crystals were redetermined using *FITATOM* (Kabsch, 1978) based on a least-squares fitting of the coordinates. Different transformations were calculated for each of the four domains (Fig. 11*a*). Slightly differing orienta-

	Intra-Dimer Angle			R	T	R	T
	LG2	SEB	SF9	DR1-LG2 =====> DR1SEB		DR1-LG2 =====> DR1-SF9	
α_1	178.6	179.3	174.9	.9994 -.0217 .0250 -.0059 -.8603 -.5097 .0325 .5092 -.8600	25.3 108.6 78.1	.2914 .7604 .5803 -.5874 -.3365 .7360 .7550 -.5554 .3486	-61.1 12.2 -9.8
α_2	178.6	179.8	178.0	.9999 -.0085 .0001 -.0072 -.8544 -.5194 .0045 .5194 -.8545	27.2 109.4 77.9	.3009 .7411 .6001 -.5801 -.3572 .7320 .7569 -.5684 .3225	-62.7 12.7 -7.7
β_1	179.4	179.2	175.4	.9993 -.0220 .0293 -.0040 -.8612 -.5083 .0364 .5078 -.8607	25.0 108.7 78.0	.3015 .7355 .6066 -.6131 -.3376 .7141 .7301 -.5873 .3492	-63.5 14.6 -9.1
β_2	178.6	179.5	178.8	.9997 -.0256 -.0059 -.0251 -.8663 -.4989 .0076 .4988 -.8666	28.4 108.2 79.2	.2877 .7451 .6017 -.6026 -.3474 .7184 .7443 -.5693 .3490	-63.0 14.5 -9.9

(*a*)

domain fit is based on ↓	R.M.S (Å) fit for each domain			
	α_1	α_2	β_1	β_2
α_1	0.83	0.82	0.97	1.13
α_2	0.86	0.73	1.04	1.02
β_1	0.87	1.03	0.92	1.58
β_2	1.14	1.15	0.92	0.83

(*b*)

Fig. 11. (*a*) Domain by domain transformations relating four domains (α_1, α_2, β_1, β_2) of the six DR1 α,β heterodimers in all three crystals determined using *FITATOM* (Kabsch, 1978). Within a crystal, only the rotation angles are specified. Between crystals, rotation matrices (R) and translation vectors in orthogonal Å (T) are specified. (*b*) Domain by domain r.m.s. fit between the Cα atoms of two heterodimers in the asymmetric unit of the DR1-LG2 crystal form.

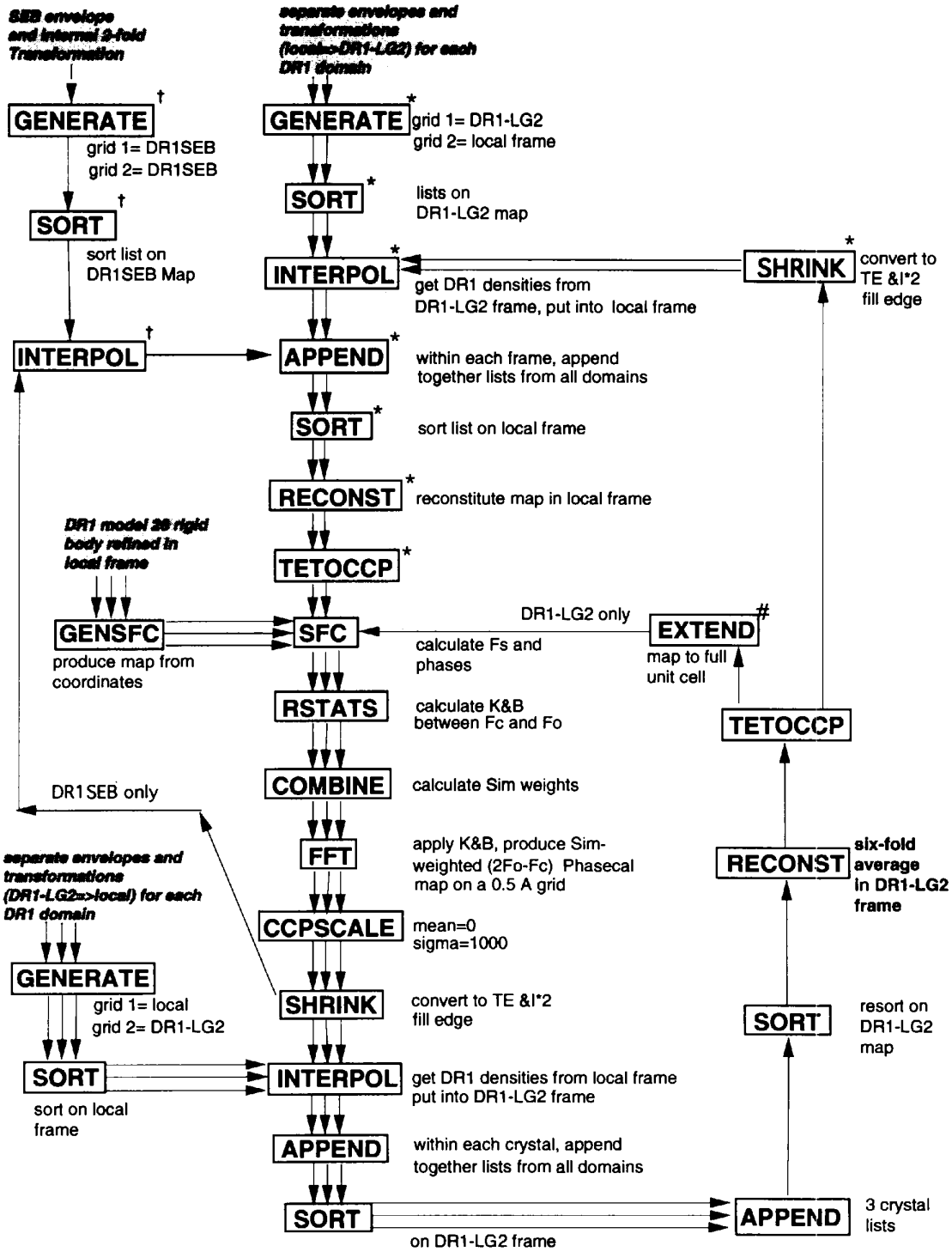

(*a*)

Fig. 12. The flow chart of programs used to iteratively sixfold average electron-density maps from the DR1-LG2 ($C222_1$) crystal form, the DR1SEB ($P2_12_12_1$) crystal form, and the DR1SF9 ($P4_32_12$) crystal form. Here (as opposed to Figs. 7 and 8) averaging is performed only in the $C222_1$ DR1-LG2 frame (see text). Also, separate envelopes and transformations are used for separate domains. The programs in boxes are either from *CCP*4, *Joy of Skewing* (Bricogne, 1976), or unpublished work. † indicates input or programs used only in the DR1SEB frame, # only in the DR1-LG2 frame, * only in the DR1SEB and DR1-SF9 frames. Shaded statements describe input into first cycle. Abbreviations are as for Fig. 7.

tions for the domains in the different crystal environments were noted (Fig. 11*b*). The r.m.s. deviation between the β_2 domains consistently tended to be higher than between the other domains.

The procedure used to iteratively sixfold average DR1 to 3.3 Å resolution (Fig. 12*a*), which relied on combining model-derived phase information for three different crystals, differed somewhat from the previously described four- and twofold averaging procedures (Fig. 7). The previous averaging step was performed in each crystal frame, and fine (0.5 Å) map grids were used for all interpolations (eight-point linear). For the sixfold averaging, however, the averaging step was performed only in the DR1-LG2 frame (Fig. 12, right column) and this averaged map was skewed over to and back-transformed in each of the crystal frames (Fig. 12, left columns). This afforded savings both in computer time and file management. In this scheme, however, the (eight-point linear) interpolation was performed from a 'coarse' 1 Å (sixfold averaged) map into the DR1SEB and DR1-SF9 frames for subsequent back-transformation. Visual inspection of such a 3.3 Å resolution map before and after this 'coarse to coarse' interpolation indicated no apparent difference.

The sixfold averaging procedure was iterated nine times to convergence (Figs. 13*a* and 13*b*) resulting in *R* factors between the back transform of the final averaged map and the DR1-LG2, DR1-SF9 and DR1SEB cryogenic data sets of 30.6, 29.6 and 30.3%, respectively.* A series of eight sixfold iteratively averaged omit maps (Sussman, Holbrook, Warrant, Church & Kim, 1978) were calculated, in which approximately 1/8th of the model was omitted in each case. Only nine of 371 amino-acid residues showed no side-chain density. Two incorrectly built loops were clearly identified by the averaging procedure, even without omitting them (Fig. 14). Averaging thus appears to provide an alternative to the use of omit maps (Blum, 1990) for overcoming model bias. The model described here has been further refined both in the DR1-SF9 (Stern *et al.*, 1994) and DR1SEB (Jardetzky *et al.*, 1994) crystal forms.

Crystal packing

The DR1 molecule is a heterodimer of α and β chains, each composed of two domains, α_1, α_2 and β_1, β_2 (Fig. 15*a*). Although the tertiary structure of the α_1, β_1 and α_2, β_2 pairs are essentially identical, like the class I HLA (Bjorkman *et al.*, 1987*a*), the overall structure is not a symmetric heterodimer. Instead, although the α_1 and β_1 domains are related by an approximate twofold symmetric axis, α_2 is related to β_2 by a screw axis with a 174° rotation and 14 Å translation.

In all three crystal forms studied here HLA–DR1 $\alpha\beta$ heterodimers are found packed into the same parallel dimer of heterodimers (Fig. 15*b*). The dimer is described as parallel because the membrane anchors (C termini) of all four chains are at one end (bottom, Fig. 15*b*) and the peptide-binding sites where T-cell recognition occurs are at the opposite end (top, Fig. 15*b*). There is no published evidence that we are aware of indicating that class II molecules are dimers either on membranes or when soluble, and our efforts to find dimers of soluble HLA–DR1 by chemical crosslinking and gel-filtration experiments were negative (Stern, unpublished work). A three-dimensional profile analysis (Lüthy, Bowie & Eisenberg, 1992) of DR1 as a monomer or dimer, shows only a marginal difference in 'profile score' between the monomer (121.85) and the dimer (124.64), providing no evidence for or against the dimer.

We have, therefore, examined the crystal packing of DR1 in the different crystal forms for other similarities. All DR1 crystals to date yielding high-resolution data have been grown in low salt, pH 4.0 to 6.0, with high concentrations (>15%) of PEG 8000. The three crystals used to determine the structure share one ~ 96 Å unit-cell axis, which is a crystallographic twofold screw axis. Packing along the 96 Å axis is similar in all three crystals (Fig. 16) and includes a crystallographic contact between dimers of $\alpha\beta$ heterodimers (buried solvent-accessible surface = 960 Å^2) as well as the non-crystallographic contact between the $\alpha\beta$ heterodimers within the parallel dimer (1300 Å^2, probe radius = 1.4 Å) (Brown *et al.*, 1993). Other molecular contacts are not shared among the three crystal forms. Very recently, a fourth crystal form (Kim, Urban, Strominger & Wiley, 1994) of DR1, this time complexed with the superantigen TSST-1, has been grown under similar conditions. This fourth form again contains the parallel DR1 dimer, but does not

* In addition to its dependence upon the quality of the data and averaging, the *R* factor was positively correlated with the number of crystal data sets used in averaging. For example, the final converged *R* factor of the DR1-LG2 cryogenic 3.3 Å data set was only 18.9% with the back-transformed one-crystal twofold-averaged electron-density map, 28.0% with a two-crystal fourfold averaged map, and 30.6% with the three-crystal sixfold averaged map. Modification of calculated electron density was restrained not only by the DR1-LG2 data set, but also by the other data sets (those of DR1-SF9 and DR1SEB). Thus, the *R* factor between the back-transformed sixfold-averaged electron-density map and any one data set could not be reduced as far. The electron-density map, though, is more readily interpretable. This is also a common phenomenon in reciprocal-space refinement of an atomic model at medium resolution where the addition of various geometrical and even non-crystallographic (Tulinsky & Blevins, 1986) restraints generally result in an improved molecular model despite higher nominal *R* factors. The averaging equivalent of a free *R* factor Brünger (1992) can be calculated. When twofold averaging was performed within the map from the DR1-LG2 data set, the *R* factor of the averaged map calculated against omitted DR1-SF9 data dropped from 42.0 to 40.8% (as opposed to 18.9% for the included DR1-LG2 data set), yielding an unbaised quantitative measure of the improvement obtained by averaging. A more convenient method of testing the course of an averaging experiment might be to omit a small random portion of the data set from recombination and map calculation and simply use it to compute a 'free' *R* factor with the back-transformed averaged map; one might expect a faulty averaging procedure to show no drop or possibly even a rise in this free *R* factor, even as the 'working' *R* factor would tend to lower during convergence.

contain the 96 Å screw axis nor does it form any crystallographic contacts with other DR1 dimers, including the one described for the other three crystals. Besides the DR1:DR1 dimer contact, the crystal is held together by contacts between TSST-1 and TSST-1, and TSST-1 and DR1. [Another DR1–LG2 crystal grown at different conditions (high salt, 2 *M* NaCl) also does not contain a 96 Å screw axis. Unfortunately diffraction is only recordable to 7 Å resolution, with poor merging statistics, and rotation-function calculations with either the DR1 monomer or dimer are inconclusive.] Taken together, the observation of the parallel dimer of DR1 α, β heterodimers in independent crystal environments argues that it is not merely a crystal artifact, but is an intrinsic property of HLA-DR1 at very high concentrations and in the crystallization conditions employed. Conclusions concerning the aggregation state of HLA-DR1 can also be extended to certain other HLA–DR alleles which crystallize in the same space group as DR1–LG2 (Gorga *et al.*, 1991).

If the parallel dimer of DR1 discovered here is not simply a crystallographic artifact, it may indicate the capacity of DR1 molecules to form dimers, possibly of such low affinity that they have escaped detection by solution studies. Whether such putative dimers might occur on the two-dimensional surface of membranes

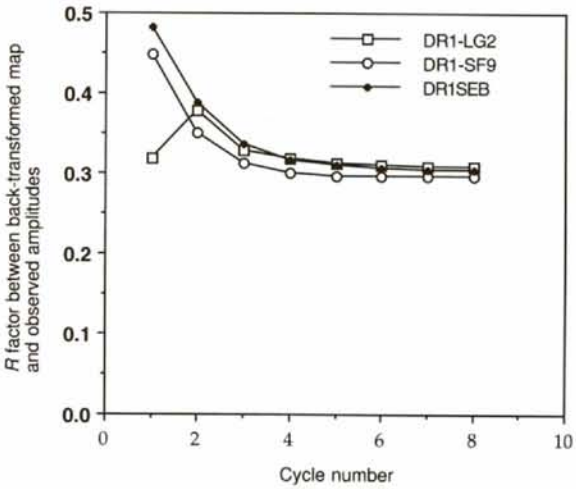

(*a*)

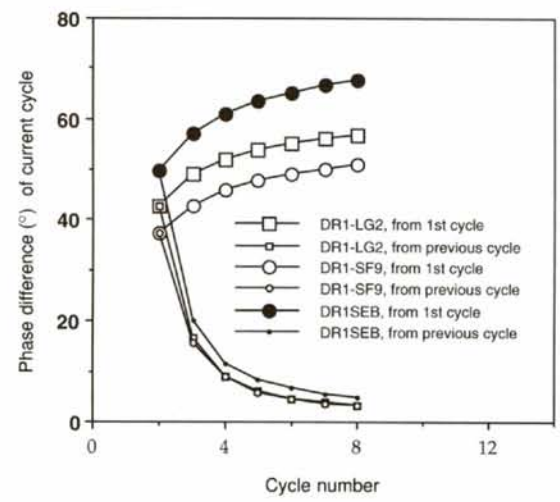

(*b*)

Fig. 13. (*a*) Statistics from a sample 'sixfold' averaging experiment where residues α38–α82 are omitted in each of six DR1 heterodimers of the three crystals. DR1 density is averaged sixfold, SEB density twofold. In the DR1-LG2 frame the model was subject to a simulated-annealing refinement protocol to remove bias. In the other frames, the model was only rigid-body refined to the data (*i.e.* never positionally refined), thus explaining their higher initial *R* factors. (*b*) Phase changes in the 'sixfold' averaging experiment.

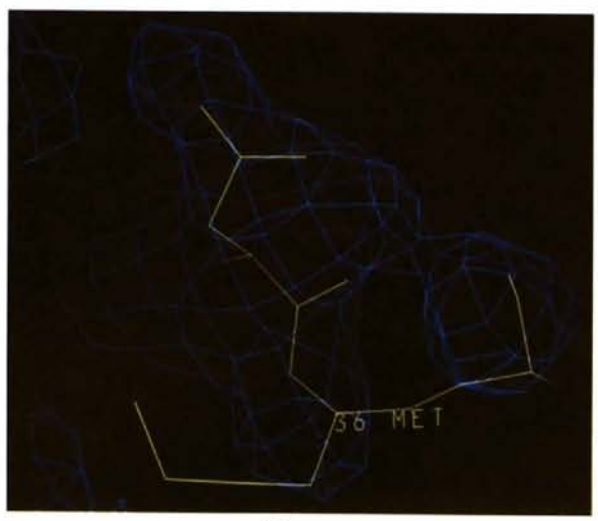

(*a*)

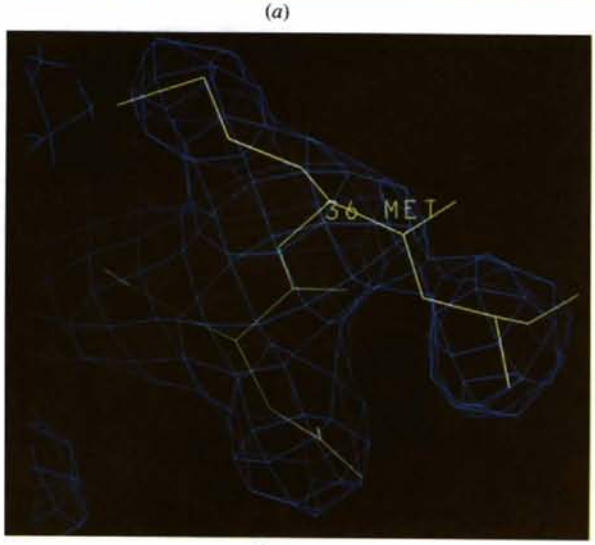

(*b*)

Fig. 14. Removal of model bias in the 3.3 Å iteratively 'sixfold' averaged electron-density map. Initial phases for the map shown were obtained with atomic models *including* the loop containing α36 as shown in (*a*). Even without omitting the residues, the sixfold averaging procedure yields a map which clearly indicates the correct path for the loop (*b*).

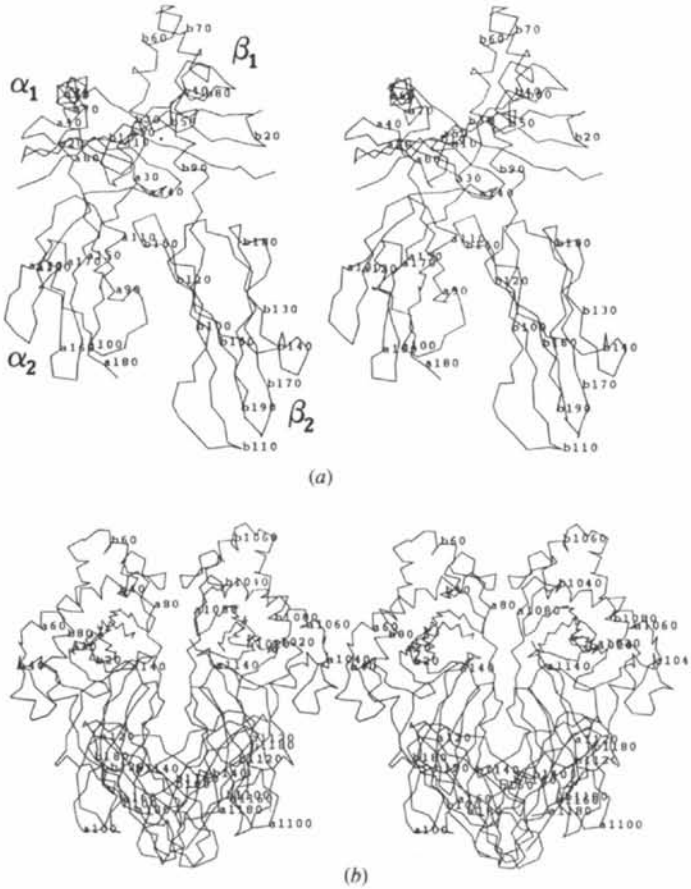

Fig. 15. (*a*) Stereo plot of the Cα atoms of the DR1 model built into the 3.3 Å sixfold averaged omit maps. The α_1 and β_1 domains are at the top; the α_2 and β_2 domains at bottom. In this view the lengths of the helices of the α_1 and β_1 domains are approximately perpendicular to the plane of the page. (*b*) Stereo plot of the Cα atoms of the parallel dimer of DR1 α, β heterodimers. This view is approximately 90° rotated about the vertical axis of the page relative to (*a*) such that the lengths of the helices of the α_1 and β_1 domains (still at top of figure) are now approximately within the plane of the page.

Pair of dimers of α,β heterodimers

is the maximum structure common to the three DR1 crystals

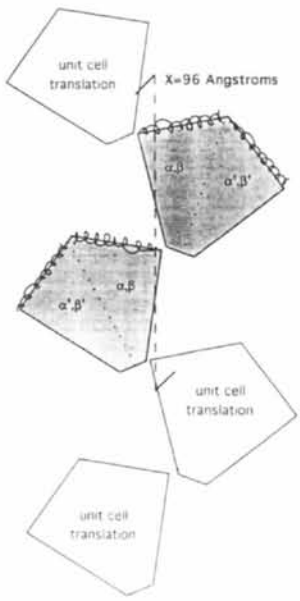

Fig. 16. Packing arrangement of DR1 molecules common to the DR1-LG2, DR1SEB and DR1SF9 crystal forms. The five-sided figure corresponds to a parallel dimer of DR1 α, β heterodimers with the dotted lines representing the local twofold symmetry axis relating individual heterodimers. The helical drawings correspond to the peptide-binding domains. The shaded figures represent the pair of parallel dimers (of heterodimers) which are related to each other by the crystallographic 96 Å long twofold screw axis. The interaction between the parallel dimers within a pair are repeated along the *x* direction by unit-cell translations. Recently, a fourth crystal form of DR1, complexed with the superantigen TSST-1 and not containing a 96 Å twofold screw axis (Kim, Urban, Strominger & Wiley, 1994) has been grown; the parallel DR1 dimer of α, β heterodimers is still observed, but crystallographic contacts between dimers, including the pair depicted in this figure, are absent.

independently, or only in the presence of other bound protein molecules is a subject of speculation. Because crosslinking of T-cell receptors may be required for initiating the intracellular signaling that leads to T-cell activation (Klinman, 1972; Janeway *et al.*, 1989), and because signaling through class II MHC molecules into antigen-presenting cells (Koulova, Clark, Shu & DuPont, 1991; Nabavi *et al.*, 1992; Schwartz, 1992; Watts, Alaverdi, Wade & Linsley, 1993) could be initiated by crosslinking the DR1 cytoplasmic domains, a role for the putative DR1 dimer has been proposed in which it forms part of a structure to initiate crosslinking events on cell surfaces (Brown *et al.*, 1993; Germain, 1993). Whether the capacity to form dimers might be part of this or some other physiological mechanism such as the recycling or disposal of empty class II molecules (Germain & Hendrix, 1991) or the intracellular transport and peptide loading of class II molecules or whether the dimers are simply an artifact of the crystallization conditions is currently unknown.

We thank P. Klimovitsky, A. Haykov and M. Frayser for technical assistance; K. Svenson, assisted by M. Pietras, for the large-scale production of tissue-cultured cells; M. Blum for helpful discussions on averaging; and other members of our group and the CHESS synchrotron staff for assistance with X-ray data collection. JHB was supported by the Howard Hughes Medical Institute, TSJ by the Cancer Research Institute, JCG by the Juvenile Diabetes Foundation International, LJS by a Damon Runyon–Walter Winchell Cancer Fellowship and the Howard Hughes Medical Institute, JLS by the NIH. DCW is an investigator with the Howard Hughes Medical Institute.

References

BJORKMAN, P. J., SAPER, M. A., SAMRAOUI, B., BENNETT, W. S., STROMINGER, J. L. & WILEY, D. C. (1987*a*). *Nature (London)*, **329**, 506–512.

BJORKMAN, P. J., SAPER, M. A., SAMRAOUI, B., BENNETT, W. S., STROMINGER, J. L. & WILEY, D. C. (1987*b*). *Nature (London)*, **329**, 512–518.

BLUM, M. L. (1990). PhD thesis, Harvard Univ., CT, USA.

BLUM, M., METCALF, P., HARRISON, S. C. & WILEY, D. C. (1987). *J. Appl. Cryst.* **20**, 235–242.

BRICOGNE, G. (1976). *Acta Cryst.* A**32**, 832–847.

BROWN, J. H. (1991). PhD thesis, Harvard Univ., CT, USA.

BROWN, J. H., JARDETZKY, T. S., GORGA, J. C., STERN, L. J., URBAN, R. G., STROMINGER, J. L. & WILEY, D. C. (1993). *Nature (London)*, **364**, 33–39.

BROWN, J. H., JARTEZKY, T., SAPER, M. A., SAMRAOUI, B., BJORKMAN, P. J. & WILEY, D. C. (1988). *Nature (London)*, **332**, 845–850.

BRÜNGER, A. T. (1990). *X-PLOR Version* 2.1, *Manual*. Yale Univ., New Haven, CT, USA.

BRÜNGER, A. T. (1992). *Nature (London)*, **332**, 472–475.

CHICZ, R. M., URBAN, R. G., LANE, W. S., GORGA, J. C., STERN, L. J., VIGNALI, D. A. A. & STROMINGER, J. L. (1992). *Nature (London)*, **358**, 764–768.

COLLABORATIVE COMPUTATIONAL PROJECT, NUMBER 4 (1994). *Acta Cryst.* D**50**, 760–763.

CROWTHER, R. A. (1972). In *The Molecular Replacement Method*, edited by M. G. ROSSMAN. New York: Gordon and Breach.

CROWTHER, R. A. & BLOW, D. M. (1967). *Acta Cryst.* **23**, 544–548.

DURBIN, R. M., BURNS, R., MOULAI, J., METCALF, P., FREYMANN, D., ANDERSON, J. E., HARRISON, S. C. & WILEY, D. C. (1986). *Science*, **232**, 1127–1132.

FITZGERALD, P. M. D. (1988). *J. Appl. Cryst.* **21**, 273–278.

FREMONT, D. H., MATSUMURA, M., STURA, E. A., PETERSON, P. A. & WILSON, I. A. (1992). *Science*, **257**, 919–927.

GARRETT, T. P. J., SAPER, M. A., BJORKMAN, P. J., STROMINGER, J. L. & WILEY, D. C. (1989). *Nature (London)*, **342**, 692–696.

GERMAIN, R. N. (1993). *Curr. Biol.* **3**, 586–589.

GERMAIN, R. N. & HENDRIX, L. R. (1991). *Nature (London)*, **353**, 134–139.

GERMAIN, R. N. & MARGULIES, D. H. (1993). *Ann. Rev. Immunol.* **11**, 403–450.

GORGA, J. C., BROWN, J. H., JARDETZKY, T., WILEY, D. C. & STROMINGER, J. L. (1991). *Res. Immunol.* **142**, 401–407.

GORGA, J. C., HOREJSÍ, V., JOHNSON, D. R., RAGHUPATHY, R. & STROMINGER, J. L. (1987). *J. Biol. Chem.* **262**, 16087–16094.

GUO, H.-C., JARDETZKY, T. S., GARRETT, T. P. J., LANE, W. S., STROMINGER, J. L. & WILEY, D. C. (1992). *Nature (London)*, **360**, 364–366.

HARRISON, S. C. (1968). *J. Appl. Cryst.* **1**, 84–90.

JANEWAY, C. A. JR, DIANZANI, U., PORTOLES, P., RATH, S., REICH, E.-P., ROJO, J., VAGI, J. & MURPHY, D. P. (1989). *Cold Spring Harbor Symp. Quant. Biol.* **LIV**, 657–666.

JARDETZKY, T. S., BROWN, J. H., GORGA, J. C., STERN, L. J., URBAN, R. G., CHI, Y.-I., STAUFFACHER, C., STROMINGER, J. L. & WILEY, D. C. (1994). *Nature (London)*, **368**, 711–718.

JONES, T. A. (1978). *J. Appl. Cryst.* **11**, 268–272.

KABSCH, W. (1978). *Acta Cryst.* A**34**, 827–828.

KAUFMAN, J. F., AUFFRAY, C., KORMAN, A. J., SHACKELFORD, D. A. & STROMINGER, J. L. (1984). *Cell*, **36**, 1–13.

KIM, J., URBAN, R. G., STROMINGER, J. L. & WILEY, D. C. (1994). *Science*, **266**, 1870–1874.

KLINMAN, N. R. (1972). *J. Exp. Med.* **136**, 241–260.

KOULOVA, L., CLARK, E. A., SHU, G. & DUPONT, B. (1991). *J. Exp. Med.* **173**, 759–762.

LOEBERMANN, H., TOKUOKA, R., DEISENHOFER, J. & HUBER, R. (1984). *J. Mol. Biol.* **177**, 531–556.

LÜTHY, R., BOWIE, J. U. & EISENBERG, D. (1992). *Nature (London)*, **356**, 83.

MADDEN, D. R., GARBOCZI, D. N. & WILEY, D. C. (1993). *Cell*, **75**, 693–708.

MADDEN, D. R., GORGA, J. C., STROMINGER, J. L. & WILEY, D. C. (1991). *Nature (London)*, **353**, 321–325.

MADDEN, D. R., GORGA, J. C., STROMINGER, J. L. & WILEY, D. C. (1992). *Cell*, **70**, 1035–1048.

MADDEN, D. R. & WILEY, D. C. (1992). *Curr. Opin. Struct. Biol.* **2**, 300–304.

METCALF, P., BLUM, M., FREYMANN, D., TURNER, M. & WILEY, D. C. (1987). *Nature (London)*, **325**, 84–6.

NABAVI, N., FREEMAN, G. J., GAULT, A., GODFREY, D., NADLER, L. M. & GLIMCHER, L. H. (1992). *Nature (London)*, **360**, 266-268.

NEPOM, G. T. & ERLICH, H. (1991). *Ann. Rev. Immunol.* **9**, 493–525.

RAO, S. N., JIH, J. & HARTSUCH, J. A. (1980). *Acta Cryst.* A**36**, 878–884.

SAPER, M. A., BJORKMAN, P. J. & WILEY, D. C. (1991). *J. Mol. Biol.* **219**, 277–319.

SCHWARTZ, R. H. (1992). *Cell*, **71**, 1065–1068.

SILVER, M. L., GUO, H.-C., STROMINGER, J. L. & WILEY, D. C. (1992). *Nature (London)*, **360**, 367–369.

STERN, L. J., BROWN, J. H., JARDETZKY, T. S., GORGA, J. C., URBAN, R. G., STROMINGER, J. L. & WILEY, D. C. (1994). *Nature (London)*, **368**, 215–221.

STERN, L. J. & WILEY, D. C. (1992). *Cell*, **68**, 465–477.

STUART, D. & ARTYMIUK, P. (1985). *Acta Cryst.* A**40**, 713–716.

SUSSMAN, J. L., HOLBROOK, S. R., WARRANT, R. W., CHURCH, G. M. & KIM, S.-H. (1978). *J. Mol. Biol.* **123**, 607–630.
TENG, T.-Y. (1990). *J. Appl. Cryst.* **23**, 387–391.
TERWILLIGER, T. C. & EISENBERG, D. (1983). *Acta Cryst.* A**39**, 813–817.
TULINSKY, A. & BLEVINS, R. A. (1986). *Acta Cryst.* B**42**, 198–200.
WATTS, T. H., ALAVERDI, N., WADE, W. F. & LINSLEY, P. S. (1993). *J. Immunol.* **150**, 2192–2202.
ZHANG, W., YOUNG, A. C. M., IMARAI, M., NATHENSON, S. G. & SACCHETTINI, J. C. (1992). *Proc. Natl Acad. Sci. USA*, **89**, 8403–8407.